Supplementary Material 1

1 Probability of activation of a gene

If $c(t)$ is the concentration of a Transcription Factor (TF) in the nucleus, the probability that the TF successful binds to the promoter site of a gene at time $t + \Delta t$ and active it (state *on*) is:

$$p^{on}(t+\Delta t) = p^{on}(t) + k_1 c(t) \cdot p^{off}(t)\Delta t - k_{-1} p^{on}(t)\Delta t + o(\Delta t) \qquad (1)$$

where $p^{off}(t)$ is the probability that the gene is inactive (state *off*) at time t, k_1 is the rate constant of transition from state *off* to state *on*, k_{-1} is the rate constant of transition from state *on* to state *off*, and $o(\Delta t)$ is a random function of Δt such that $\frac{o(\Delta t)}{\Delta t} \to 0$ when $\Delta t \to 0$.

Eq. (1) is the master equation for the process of transition from state 0 to state 1 for a single gene due to the binding of a TF to its promoter.

Dividing Eq. (1) by Δt and calculating the limit when $\Delta t \to 0$ we obtain:

$$\lim_{\Delta t \to 0} \frac{p^{on}(t+\Delta t) - p^{on}(t)}{\Delta t} = k_1 c(t) \cdot p^{off}(t) - k_{-1} p^{on}(t) + \lim_{\Delta t \to 0} \frac{o(\Delta t)}{\Delta t} \qquad (2)$$

which leads to:

$$\frac{dp^{on}(t)}{dt} = k_1 c(t) \cdot p^{off}(t) - k_{-1} p^{on}(t) \qquad (3)$$

Assuming that the binding of the TF to the promoter site is a Bernoulli process: $p^{on}(t) + p^{off}(t) = 1$, and we finally obtain:

$$\frac{dp^{on}(t)}{dt} = k_1 c(t) \cdot \left(1 - p^{on}(t)\right) - k_{-1} p^{on}(t) \qquad (4)$$

2 Probability of inhibition of a gene

The presence of a competitive inhibitor of the TF activity, which not necessarily acts on the same promoter site, can be modeled as:

$$\frac{dp^{on}(t)}{dt} = \frac{k_1 c(t)}{inh(t) + \gamma} \cdot \left(1 - p^{on}(t)\right) - k_{-1} p^{on}(t) \qquad (5)$$

where $inh(t)$ is the concentration of the inhibitor in the nucleus, and γ is a constant. Expression (5) corresponds to Eqs. 5-8 of main text.

Supplementary Material 2

3 Stability analysis of nonlinear systems

Cells are complex networks of physicochemical processes that support a highly organized structure and function. Thus, each cellular process sustained by a cell involves different levels of cellular organization. Every level cellular level of organization can be represented as a subsystem (subnetwork) with modular. In this form, cells can be modeled as formed by a set of subsystems like the gene regulatory network (GRN), the network of synthesis and distribution of proteins, the network of signaling pathways, and the metabolic network, among others. The information flow through the set of cellular subsystems that controls the cell response to environmental signals occurs according to the canonical schema of SM 2 Figure 1. DNA or RNA viruses can drastically modify this flow of information.

An important remark from SM 2 Figure 1 is that the flow of information through cellular subsystems is due to a continuous flow of matter and energy, according to the respective laws of conservation. Taking into account the flow of matter at each point of the cell, the respective mass balance equation is:

$$\frac{\partial c_k(\mathbf{x},t)}{\partial t} = \sum_r \nu_{rk} \cdot \omega_r \left(c_1(\mathbf{x},t) c_2(\mathbf{x},t) ... c_k(\mathbf{x},t) ... c_s(\mathbf{x},t) \right) + D_k \nabla^2 c_k(\mathbf{x},t) \qquad (1)$$

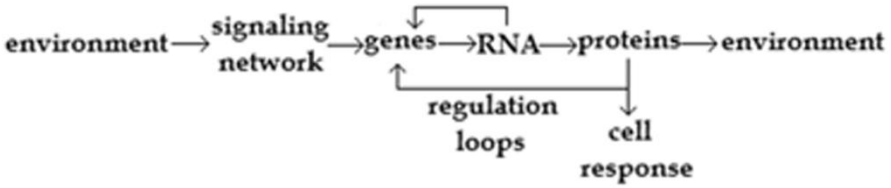

SM 2 Figure 1.- Flow of information between cell subsystems. Changes in environmental conditions are sensed by cell signaling networks, which code and transmit this information to the nucleus. Coded information is decoded by the transcription machinery that, in response to this information, activates and inactivates a set of specific genes, giving rise to a specific distribution of effectors proteins. These proteins are responsible for the cell specific response to the environmental conditions. Some of these proteins can be used to regulate gene expression, acting as specific transcription factors that form complex regulatory loops inside the nucleus. Proteins can also be secreted to modify the cell environment. Viral RNA and DNA can modify this flow of information by acting directly on the cell genome, drastically modifying the population of effectors proteins and their function.

Equation (1) means that the local rate of variation of the concentration of the substance *k* (denoted by c_k) at point **x** at time *t* is equal to the net rate of diffusion of *k* inside the cell volume *V* (denoted by $D_k \nabla^2 c_k(\mathbf{x},t)$) plus the rate of formation/degradation of *k* due to the local chemical reactions inside *V*. In Eq. (1), ω_r represents the local rate of the chemical reaction *r*, which is a functional of the concentration of the reactive substances at point **x** at time *t*, and ν_{rk} is the stoichiometric coefficient of *k* in reaction *r*.

The reaction term of Eq. (1) can be rewritten as:

$$\sum_{\substack{r \\ k=1,2,...,s}} \nu_{rk} \cdot \omega_r \left(c_1(\mathbf{x},t)c_2(\mathbf{x},t)...c_k(\mathbf{x},t)...c_s(\mathbf{x},t)\right) = f_k\left(c_1(\mathbf{x},t),c_2(\mathbf{x},t),...,c_k(\mathbf{x},t),...c_s(\mathbf{x},t)\right) \quad (2)$$

leading to:

$$\frac{\partial c_k(\mathbf{x},t)}{\partial t} = f_k\left(c_1(\mathbf{x},t),c_2(\mathbf{x},t),...,c_k(\mathbf{x},t),...c_s(\mathbf{x},t)\right) + D_k\nabla^2 c_k(\mathbf{x},t) \quad k=1,2,...,s \quad (3)$$

which is the well known form of the reaction-diffusion equation for the substance *k*. It indicates that the temporal variation of the concentration of *k* at point **x** at time *t* depends on the balance between the chemical processes in which this substance takes part, represented by the function f_k, and its diffusion rate in the cellular medium. Function f_k is generally a nonlinear function of the concentration of the reactive substances, and Eq. (3) usually has not an analytical solution. In a homogeneous medium, the diffusive term in Eq. (3) is null, and f_k completely defines the entire system dynamics in the *s*-dimensional phase space, which is defined by the set of concentration values of the *s* reactive substances. The systems dynamics is represented by a trajectory in this space or **phase space**, defined by the column vector $\mathbf{c}(t) = \langle c_1(t)c_2(t)...c_s(t)\rangle^T$. In nonlinear systems this trajectory can have peculiar characteristics like high sensitivity to initial conditions, bifurcations and complex loops that represent a great variety of dynamical behaviors observed in biological systems like limit cycles, hysteresis, bistability, ultra sensitivity, among others. In a no homogeneous medium, the diffusive term of Eq. (3) produces a more complex dynamical behavior of the system, giving rise to phenomena like traveling waves, spirals and spatially located bursting of second messengers and proteins, among others.

The first problem concerning the dynamics of nonlinear systems is the determination the steady points of the system in the phase space.

A steady point is a column vector $\mathbf{c}^o = \langle c_1{}^o(t)c_2{}^o(t)...c_s{}^o(t)\rangle^T$ for which equation:

$$\dot{\mathbf{c}}(t) = \mathbf{f}\left(\mathbf{c}(t)\right), \text{ where } \mathbf{f}\left(\mathbf{c}(t)\right) = \begin{bmatrix} f_1\left(c_1(t),c_2(t),...c_k(t),...c_s(t)\right) \\ \vdots \\ f_s\left(c_1(t),c_2(t),...c_k(t),...c_s(t)\right) \end{bmatrix} \quad (4)$$

becomes zero. Once the set of steady points of the system is settled on, is necessary to determine their stability. Eq. (4) subject to the initial condition $\mathbf{c}(0) = \mathbf{c}_0$ defines a **nonlinear dynamical system**.

The steady point $\mathbf{c}^o$ of a dynamical system is **Liapunov stable** if for each $\varepsilon > 0$ exits a $\delta > 0$ such that $\|\mathbf{c}(t) - \mathbf{c}^o\| < \varepsilon$ whenever $\|\mathbf{c}(0) - \mathbf{c}^o\| < \delta$, i.e., any trajectory that initiates at a distance δ of the steady point $\mathbf{c}^o$ remains at a distance ε of it all time.

The steady point $\mathbf{c}^o$ of a dynamical system is attracting if exists a $\delta > 0$ such that $\lim_{t\to\infty} \mathbf{c}(t) = \mathbf{c}^o$ for any trajectory $\mathbf{c} = \mathbf{c}(t)$ whenever $\|\mathbf{c}(0) - \mathbf{c}^o\| < \delta$, i.e., any trajectory that initiates at a distance δ of the steady point $\mathbf{c}^o$ will converge to it eventually. In this case, the point $\mathbf{c}^o$ is an **attractor** of the dynamical system in the phase space. A steady point $\mathbf{c}^o$ Liapunov stable and attractor is asymptotically stable. A steady point $\mathbf{c}^o$ that is neither stable nor attractor is unstable, and is a **repulsor** in the phase space.

Generally, the nonlinear systems trajectories cannot be determined in an analytical form. However, it is possible to perform a qualitative analysis to find out the global behavior of the dynamical system in the corresponding phase space. As a vector can be assigned to each point of this space, according to Eq. (4), the vector field associated to the phase space can be drawn. By flowing this vector field, a phase point traces a solution **c**(*t*) of the dynamical system, corresponding to a trajectory winding through the phase space.

It is of importance to point out the fact that if the function **f** of Eq. (4) is continuous and all its partial derivates $\frac{\partial f_i}{\partial c_j}$ $i,j=1,2,...,s$ are also continuous in **c** for a given subset $D \subset \Re^n$, then for every $\mathbf{c}_0 \in D$ the initial value problem of Eq. (4), has solution **c**(*t*) in some time interval (-*t*,*t*) around *t* = 0 and this solution is unique. A topological implication of this theorem is that two trajectories cannot intersect and, as consequence, chaos is ruled out of any 2-dimensional phase space but arises as a possible behavior of every s-dimensional dynamical system with s > 2.

The phase space analysis of the dynamics of a nonlinear system takes into account the following aspects: 1) the number, position and stability of the steady points; 2) the arrangement of the trajectories near the steady points; and 3) the existence and stability of closed orbits.

The arrangement of the trajectories around steady points is determined by linearization of the original nonlinear system, and analysis of the behavior of the eigenvalues of the Jacobian matrix of the linearized system around each steady point. For example, considering a 2-dimensional phase space and a steady point $\mathbf{c}^o = \langle c_1^o, c_1^o \rangle^T$, a small perturbation from this steady state drives the nonlinear dynamical system $\begin{bmatrix} \dot{c}_1(t) \\ \dot{c}_2(t) \end{bmatrix} = \begin{bmatrix} f_1(c_1(t), c_2(t)) \\ f_2(c_1(t), c_2(t)) \end{bmatrix}$ into a new trajectory $\delta\mathbf{c}(t) = \langle \delta c_1(t), \delta c_2(t) \rangle^T$, where $\delta c_1(t) = c_1(t) - c_1^o$, and $\delta c_2(t) = c_2(t) - c_2^o$. In this form:

$$\begin{aligned} \delta\dot{c}_1 = \dot{c}_1 &= f_1(c_1^o, c_2^o) + \left.\frac{\partial f_1}{\partial c_1}\right|_{(c_1^o, c_2^o)} \delta c_1 + \left.\frac{\partial f_1}{\partial c_2}\right|_{(c_1^o, c_2^o)} \delta c_2 + O\left(\delta^2 c_1, \delta^2 c_2, \delta c_1 \delta c_2\right) \\ &= \left.\frac{\partial f_1}{\partial c_1}\right|_{(c_1^o, c_2^o)} \delta c_1 + \left.\frac{\partial f_1}{\partial c_2}\right|_{(c_1^o, c_2^o)} \delta c_2 + O\left(\delta^2 c_1, \delta^2 c_2, \delta c_1 \delta c_2\right) \text{ because } f_1(c_1^o, c_2^o) = 0 \end{aligned} \tag{5}$$

in a similar form:

$$\delta\dot{c}_2 = \dot{c}_2 = \left.\frac{\partial f_2}{\partial c_1}\right|_{(c_1^o, c_2^o)} \delta c_1 + \left.\frac{\partial f_2}{\partial c_2}\right|_{(c_1^o, c_2^o)} \delta c_2 + O\left(\delta^2 c_1, \delta^2 c_2, \delta c_1 \delta c_2\right) \tag{6}$$

which leads to the linearized dynamical system:

$$\begin{bmatrix} \delta\dot{c}_1(t) \\ \delta\dot{c}_2(t) \end{bmatrix} = \begin{bmatrix} \left.\frac{\partial f_1}{\partial c_1}\right|_{(c_1^o, c_2^o)} & \left.\frac{\partial f_1}{\partial c_2}\right|_{(c_1^o, c_2^o)} \\ \left.\frac{\partial f_2}{\partial c_1}\right|_{(c_1^o, c_2^o)} & \left.\frac{\partial f_2}{\partial c_2}\right|_{(c_1^o, c_2^o)} \end{bmatrix} \begin{bmatrix} c_1(t) \\ c_2(t) \end{bmatrix} = \mathbf{J}[c_1, c_2] \begin{bmatrix} c_1(t) \\ c_2(t) \end{bmatrix} \tag{7}$$

$\mathbf{J}[c_1, c_2]$ represents the Jacobian matrix of the linearized dynamical system in Eq. (6). The eigenvalues λ_1, λ_2 of $\mathbf{J}[c_1, c_2]$ can be calculated from the characteristic equation: $|\mathbf{J}[c_1, c_2] - \lambda \mathbf{I}| = 0$. Depending on the nature of the eigenvalues, it is possible to know the arrangement of the trajectories near each steady point of the nonlinear system (SM 2 Figure 2). This linearization process can be extended to perform the phase space analysis of higher dimensional nonlinear dynamical systems.

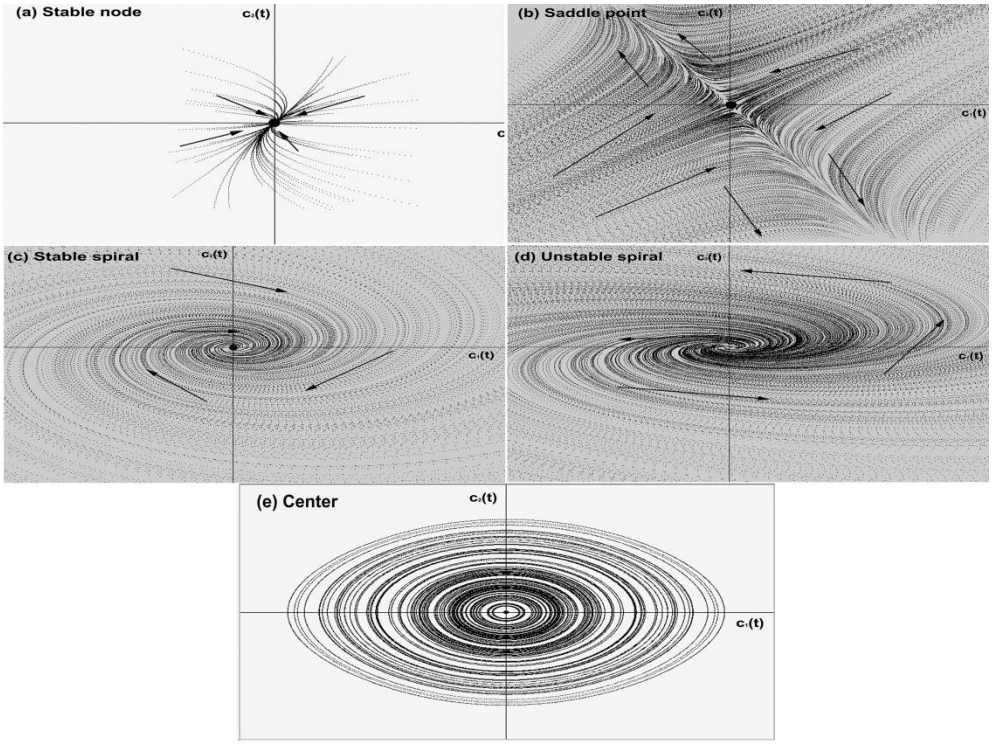

SM 2 Figure 2.- Classification of the steady points of a 2-dimensional linearized dynamical system. (a) There is a stable node or attractor in the phase space when both eigenvalues λ_1 and λ_2 are real and negative (when both eigenvalues are positive, the steady point is a unstable node or repulsor); (b) There is a saddle point in the phase space when both eigenvalues λ_1 and λ_2 are real, but one of them is positive and the other is negative. The stable manifold is spanned by the eigenvector associated to the negative eigenvalue. The unstable manifold is spanned by stable the eigenvector associated to the positive eigenvalue. (c) There is a stable spiral in the phase space when both eigenvalues λ_1 and λ_2 are complex conjugated with negative real part. (d) On the contrary, if both eigenvalues λ_1 and λ_2 are complex conjugated with positive real part the spiral is unstable. (e) When λ_1 and λ_2 are pure imaginary the steady point is a center surrounded by a series of stable closed orbits. All figures show the flow of the dynamical system in the phase space spanned by the basis conformed by the variables $c_1(t)$ and $c_2(t)$. The black point represents the steady point of the dynamical system, and the arrows mark out the direction of the flow of the vector field.

An important question that arises at this point is whether the behavior of the trajectories obtained from Eq. (7) accurately reflects the real behavior of the trajectories of the original nonlinear system.. If the linearized system has a saddle, a node or a spiral at a given steady point, then the original nonlinear system also has a saddle, a node or a spiral at that steady point. Furthermore, if a steady point is a stable saddle or node of the linearized dynamical system, then is also a stable saddle or node of the nonlinear system. In this case, the neglected nonlinear terms of Eq. (5) and Eq. (6) practically have no effect on the stability of these points when $\mathrm{Re}(\lambda) \neq 0$, for both eigenvalues. This kind of steady points is known as **hyperbolic points**, and they are not affected by the small nonlinear perturbations. The topological implication of this fact is that the vector field corresponding to a

saddle or a node is not altered by small nonlinear perturbations and, as consequence, has **structural stability**.

When the eigenvalues of the Jacobian matrix are pure imaginary $\lambda = \pm i$, the steady point is a center. The trajectories around this point are closed orbits that are stable. However, the neglected nonlinear terms in Eq. (5) and Eq. (6) can produce an imperfect closure of the orbit, giving rise to a spiral. In this form, the vector field corresponding to a center is altered by small nonlinear perturbations that transform the center into a spiral and, as consequence, has not structural stability.

According to their stability, steady points of 2-dimensional dynamical systems can be classified into a: 1) **Robust case**, which includes repellers or sources, for which both eigenvalues have Re(λ) > 0; attractors or sinks, for which both eigenvalues have Re(λ) < 0 and saddles, for which one eigenvalues has Re(λ) > 0 and the other one has Re(λ) < 0; 2) **Marginal case**, which includes centers for which both eigenvalues are pure imaginary, and non-isolated steady points for which one eigenvalue has Re(λ) = 0.

However, the phase space of a nonlinear system can exhibit another kind of closed orbits called **limit cycles**, which cannot be observed in linear systems. A limit cycle is an isolated trajectory for which neighbor trajectories can be only spirals that converge to it or diverge from it. If all the spirals converge into the limit cycle, this closed orbit is stable, otherwise is unstable. The existence of this kind of closed trajectories in the plane is settled down by the Poincaré-Bendixson theorem. According to this theorem, exits a trajectory C, which is either a closed orbit or a spiral that converges to a closed orbit as $t \to \infty$, confined inside a certain closed bounded region R of the plane. This theorem assumes 1) the existence of a vector field $\dot{\mathbf{c}} = \mathbf{f}(\mathbf{c})$ that is continuously differentiable on an open set of the plane containing R, and 2) R does not contain any fixed point. A consequence of this theorem is that in a 2-dimensional phase space any trajectory trapped into a closed bounded region R must converge to a limit cycle.

However, in higher dimensional systems the Poincaré-Bendixon theorem does not longer apply and trajectories can be trapped into a closed region of the phase space without converge into a limit cycle or settle down to a fixed point, and they could be attracted by a complex geometric object called strange attractor, which is a fractal set on which the motion is no periodic and sensitive to very small changes in initial conditions. This sensitivity makes the motion unpredictable as t increases, giving rise to a **chaotic dynamics.**

The qualitative features of the vector field of a biochemical dynamical system are strongly dependent on the set of parameters of its corresponding set of differential equations. As the value of one of these parameters changes, the qualitative features of the vector field undergo local variations around the steady points. This parameter-dependent change in the local topological structure of a vector field is known as bifurcation. They generally occur in a one-dimensional subspace, and the rest of the dimensions of the phase space are affected as consequence of the flow that can be attracted or repelled from this subspace. Taking into consideration the imaginary plane, we can roughly classify bifurcations into two cases: 1) the eigenvalues of the Jacobian matrix are both real and bifurcations occur along the real axis as certain parameter α changes. This kind of bifurcation comprises the saddle-node bifurcation; the transcritical bifurcation, and the subcritical and supercritical pitchfork bifurcation. 2) The eigenvalues of the Jacobian matrix are complex conjugated. Bifurcations occur

crossing the imaginary axis as certain parameter α changes. This kind of bifurcation comprises the supercritical and subcritical Hopf bifurcation.

In the first case, a) the saddle-node bifurcation causes local variations in the vector field around two points: a saddle and a node, as a bifurcation parameter α changes. These points become closer as parameter α varies until they collide and annihilate each other. This type of bifurcation has interesting applications in some models of biological processes that imply the presence of chemical switches; b) a transcritical bifurcation occurs when two steady points interchange their stability as the bifurcation parameter α varies; c) the normal form of an ordinary differential equation (ODE) that exhibits a subcritical pitchfork bifurcation is: $\dot{c} = \alpha c + c^3$. When α <0, there are one stable steady point at $c_1^o = 0$, and there are two unstable points at $c_{2,3}^o = \pm\sqrt{-\alpha}$. When α > 0 the only real steady point c^o = 0 becomes unstable. The normal form of an ODE that exhibits a supercritical pitchfork bifurcation is $\dot{c} = \alpha c - c^3$. When α < 0 the only real steady point c^o = 0 is stable. For α > 0 there is an unstable steady point at $c_1^o = 0$, and two stable steady points at $c_{2,3}^o = \pm\sqrt{\alpha}$.

In the second case, the presence of a Hopf bifurcation leads the system to a limit cycle. As the bifurcation parameter α varies, when a certain critical value α_c is reached the supercritical Hopf bifurcation drives the transformation of a stable spiral into an unstable spiral that converges to a stable limit cycle (SM 2 Figure 2). The case of a subcritical Hopf bifurcation is more complicated. A typical example is when an unstable limit cycle shrinks to cero amplitude as the bifurcation parameter α reaches its critical value α_c, at which the cycle engulfs the node rendering it unstable and making the system to jump to a distant attractor when $\alpha > \alpha_c$. This new attractor could be a steady point, another limit cycle, infinity or a chaotic attractor (for higher dimensional systems).

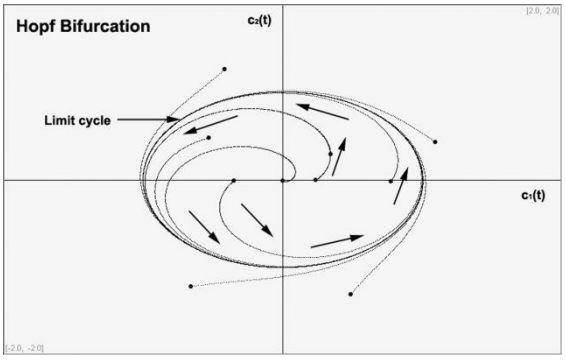

SM 2 Figure 2.- Supercritical Hopf bifurcation. This kind of bifurcation transforms a stable spiral into an unstable spiral that converges to a stable limit cycle when the value of the bifurcation parameter α reaches some critical value α_c. The black points in the figure are different initial conditions of the dynamical system. The arrows mark out the direction of the flow of the vector field. The phase space is spanned by $c_1(t)$ and $c_2(t)$.

4 Stability analysis of the model

One of the objectives of the model is to determine how the phase space of the circuit of Figure 2 of the main text is structured, i.e., how the trajectories span around the fixed points in the *n*-dimensional phase space for the set of initial conditions and parameter values. A second objective is to know in what extent this phase space structure is changed by the presence of the SARS-CoV-2 virus. The third objective is to find the possible bifurcations of the system and to identify which parameter or parameters are the responsible of this change in the qualitative dynamical behavior of the system.

The model of the circuit consist of 10 nonlinear coupled ODES that describe the dynamics of the interaction of the proteins that form the dynamical system, and four stochastic differential equations that describe the activation of the genes *NK κB, IL-6, Cox2* and *IκB* according to the feedback circuits shown in Figure 3 of main text (see also Table 1 of main text).

In this form the 10-dimensional dynamical system can be written as: $\dot{\mathbf{x}} = \mathbf{f}\left(\mathbf{x}(t)\right)$, where:

$\mathbf{x}(t) = \left[NF\kappa B(t), nf^*(t), i\kappa bnf(t), Nsp5(t), hd(t), hd^*(t), il6(t), i\kappa b(t), cox2(t), pge2(t) \right]^T$ is the state vector at time *t*, and **f** is a nonlinear function of the state vector **x**(*t*). This equation describes the trajectories of the dynamical system in the phase space. The four master equations for the temporal dynamics of the gene regulatory network (GRN) of the lung cell define the vector:

$\mathbf{x}_s(t) = \left[p^{on}_{IL6}(t), p^{on}_{I\kappa B}(t), p^{on}_{Cox2}(t), p^{on}_{NF\kappa B}(t) \right]^T$ (see Table 1 of main text). This vector describe the change in the probability distribution of the activation of each gene of the GNR, which usually converges to a steady constant distribution when $t \to \infty$. We numerically solved the model using the predictor-corrector Euler method and the Runge-Kutta 4,5 method in Math-Lab with the parameter values reported in Table 1 of main text, and for a set of 100 random initial conditions in each case.

We assume that all parameters of the model are unknown, so we define and arbitrary reference state (ARS) in which the activation of NF κB is transitory (Figure 4A in main text) in presence of an external input ($\alpha(t)$ = 10 pg mL^{-1} s^{-}1), and in absence of the SARS-CoV-2 virus.

Solution of the model for the ARF defines the stable node and the steady probability distribution:

$$\mathbf{x}^o_{ARF} = [0,0,0,0,15,120,20,0.91,0,0]$$

$$\mathbf{x}^o_s = [0,0,0,0] \qquad (13)$$

Thus, in ARS the probability of activation of all genes become zero, and the concentration of IL-6 in plasma is 20 pg mL^{-1} (see Figure SM2 3a). Thus, ARS is a state in which the external signal $\alpha(t)$ produces a sustained high concentration of the cytokine in the circuit beside the fact that NF κB is transiently switched *on* (see Eq. 12 of main text).

Perturbation of ARS with Nsp5 changes the position of the steady point without modifying its qualitative nature, as is shown in Figure SM2 3b. In this case the stable node and the steady probability distribution are:

$$\mathbf{x}^{o}_{virus} = [1.41, 5.65, 0.09, 20, 0.71, 6.71, 20.86, 0.25, 0.71, 9.79] \quad (14)$$

$$\mathbf{x}^{o}_{s} = [0.71, 0.88, 0.71, 0.71]$$

which indicate that the virus effectively induces the decrease in the concentration of free and nuclear HDAC2 (*hd* = 0.71 pg mL^{-1} and *hd** = 6.71 pg mL^{-1}) increasing the probability of activation of *NF κB* and its target genes. In particular, activation of *IL-6* does not significantly alters the steady level of IL-6 in plasma, indicating that the external signal $\alpha(t)$ is still the main cause of the high level of the cytokine in the circuit when ARS is perturbed by the viral protein Nsp5.

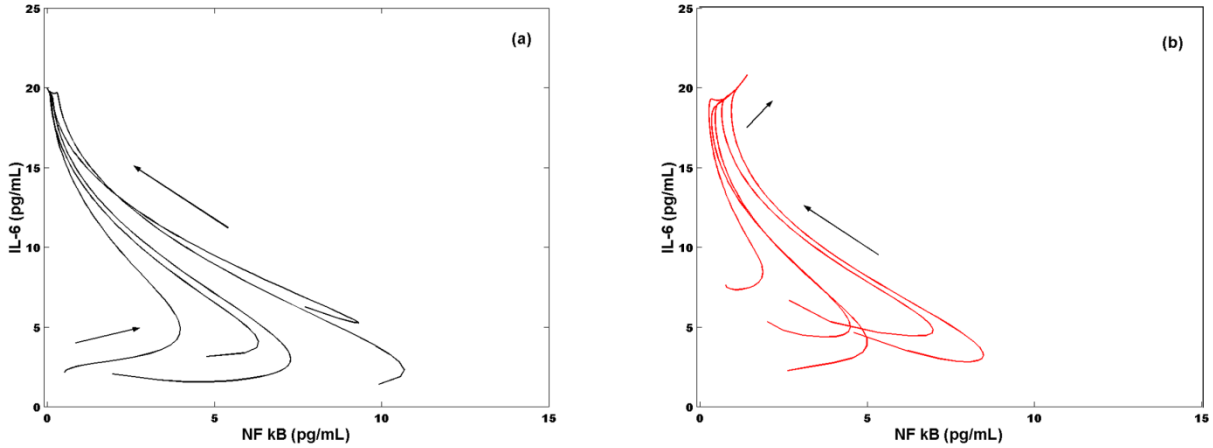

Figure SM2 3.- Viral perturbation of ARS. a) Projection of the 10-dimensional phase space of the circuit of Figure 2 of main text on the NF κB-IL-6 phase plane in the ARS. In this Figure we show only five trajectories generated from five random initial conditions that converge to the stable node $\mathbf{x}^{o}_{ARS}$ that corresponds to a state of high concentration of IL-6 (20 pg mL^{-1}) in the plasma and zero cytoplasmic free NF κB (equation 13 SM2). b) The presence of the viral protein Nsp5 changes the position of the stable node in the NF κB-IL-6 without changing its qualitative nature. For this stable node $\mathbf{x}^{o}_{virus}$ the concentration of IL-6 in plasma has a small increase but there is also a small concentration of cytoplasmic NF κB in the circuit. For both panels: $\alpha(t)$ = 10 pg mL^{-1} s^{-1}, and the parameters values are the reported in Table 1 of main text.

5 Parameter Variation

3.1) Gene Translation rate

We varied the translation rates of *NF κB*, *IL-6*, *Cox2*, and *IκB* genes to test the influence of these parameters on the circuit dynamics while the rest of the parameters remain without change with respect to their value reported in Table 1 of main text. We found that a high rate of translation of *NF κB* ($V^{\max}_{nf} = 10$ pg mL^{-1} s^{-1}), *IκB* ($V^{\max}_{I\kappa B} = 15$ pg mL^{-1} s^{-1}), and *IL-6* ($V^{\max}_{IL6} = 20$ pg mL^{-1} s^{-1}), in absence of the virus, defines a stable node and a steady probability distribution identical to the one of ARS (Figure SM2 3a and Figure SM2 4a). This result indicate that the high translation rates of *NF κB*, *IL-6*, and *IκB* are not sufficient to permanently overcome the inhibitory effect that the epigenetic regulator HDAC2 exerts on *NF κB*, when α(t) = 10 pg mL^{-1} s^{-1}. In this case, the value of the rate of translation of *Cox2* is constant (2 pg mL^{-1} s^{-1}).

In contrast, in presence of protein Nsp5 the high translation rates of *NF κB* ($V_{nf}^{\max} = 10$ pg mL^{-1} s^{-1}), *IκB* ($V_{I\kappa B}^{\max} = 15$ pg mL^{-1} s^{-1}), and *IL-6* ($V_{IL6}^{\max} = 20$ pg mL^{-1} s^{-1}) produce a stable node and a steady probability distribution:

$$\mathbf{x}_{OSIS}^{o} = [9.41, 37.65, 0.61, 20, 0.71, 5.71, 35.73, 0.31, 9.41, 7.6]$$
$$\mathbf{x}_{S}^{o} = [0.94, 0.97, 0.94, 0.94] \quad (15)$$

that correspond to a state with an elevated concentration of free cytoplasmic and nuclear NF κB (9.41 and 37.65 pg mL^{-1} respectively), a high concentration of the viral protein Nsp5 (20 pg mL-1), a low concentration of cytoplasmic and nuclear HDAC2 (0.21 and 5.71 pg mL^{-1}, respectively), and a high concentration of IL-6 in plasma (35.73 pg mL^{-1}). This state is the over stimulated immune state (OSIS) observed in critical patients of COVID19 (Figure SM2 4b) produced by a high rate of production of IL-6, and by the inhibition of HDAC2 by the viral protein Nsp5 (see main text).

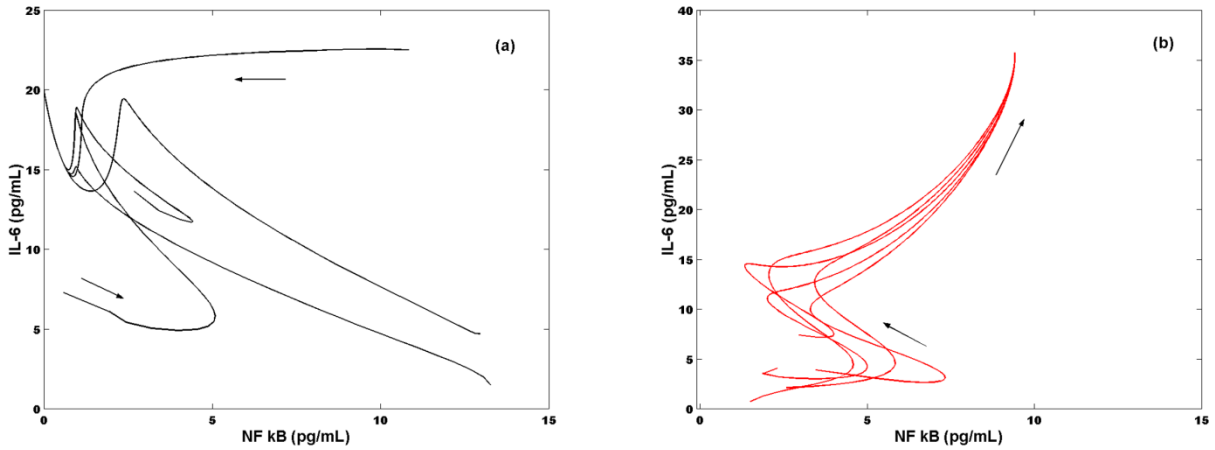

Figure SM2 4.- OSIS. a) Projection of the 10-dimensional phase space of the circuit of Figure 2 of main text on the NF κB-IL-6 phase plane for high translation rates of *NF κB*, *IL-6* and *IκB* in absence of virus. In this Figure we show only five trajectories generated from five random initial conditions that converge to the stable node that corresponds to a state of high concentration of IL-6 (20 pg mL^{-1}) in the plasma and zero cytoplasmic free NF κB (Equation 13 of SM2). b) The presence of the viral protein Nsp5 changes the position of the stable node in the NF κB-IL-6 phase plane without changing its qualitative nature. For this stable node the concentration of IL-6 in plasma is high (~ 35 pg mL^{-1}), and the concentration of cytoplasmic and nuclear HDAC2 (0.21 and 5.71 pg mL^{-1}, respectively) are lower than in ARS (Equation 13 SM2). This stable node represents the OSIS. For both panels: $\alpha(t)$ = 10 pg mL^{-1} s^{-1}, and the value of the rest of the parameters are the reported in Table 1 of main text. $V_{nf}^{\max} = 10$ pg $\cdot mL^{-1} \cdot s^{-1}$, $V_{I\kappa B}^{\max} = 15$ pg $\cdot mL^{-1} \cdot s^{-1}$, and $V_{IL6}^{\max} = 20$ pg $\cdot mL^{-1} \cdot s^{-1}$.

3.2) Rate of IL-6 release from external sources.

We analyzed the effect of different rates of IL-6 release from external sources ($\alpha(t)$) on the dynamics of the circuit of Figure 2 of main text. We varied the parameter $\alpha(t)$ from 0 to 20 pg mL^{-1} s^{-1} in presence of Nsp5. The value of the rest of the parameters are constant (Table 1 main text). In Figure SM2 5a we show that variation of $\alpha(t)$ from 0 to 20 pg mL^{-1} s^{-1} produces a series of trajectories

trapped in a narrow region of the NF κB-Il-6 phase plane, when the translation rates of all genes are equal to 2 pg mL^{-1} s^{-1}. Each trajectory converge to a stable node in which the steady concentration of cytoplasmic NF κB is ~ 1.4 pg mL^{-1}, and the steady concentration of IL-6 changes from 5 to 40 pg mL^{-1} according to the value of α. The circuit becomes unstable for $\alpha(t)$ > 50 pg mL^{-1}.

In OSIS $V_{nf}^{\max} = 10$ pg mL^{-1} s^{-1}, $V_{i\kappa B}^{\max} = 15$ pg mL^{-1} s^{-1}, and $V_{IL6}^{\max} = 20$ pg mL^{-1} s^{-1}. The rest of the parameters have the value indicated in Table 1 of main text. When α varies from 0 to 20 pg mL^{-1} s^{-1} the trajectories span inside a wider region of the NF κB-IL-6 phase plane and each one converge to a stable node with a steady concentration of NF κB of ~ 10 pg mL^{-1}, and a steady concentration of Il-6 that varies from a minimum of ~ 20 pg mL^{-1} to ~ 55 pg mL^{-1} (Figure SM 2 5b) , which are values higher that the shown in panel (a) of the same figure. These results indicate that the viral protein Nsp5 effectively amplifies the effect of the external signal α, increasing the levels of free NF κB and IL-6 in the circuit. When α = 1 pg mL^{-1} s^{-1}, the circuit exhibits a tremor in the trajectory that disappears before entering the stable node.

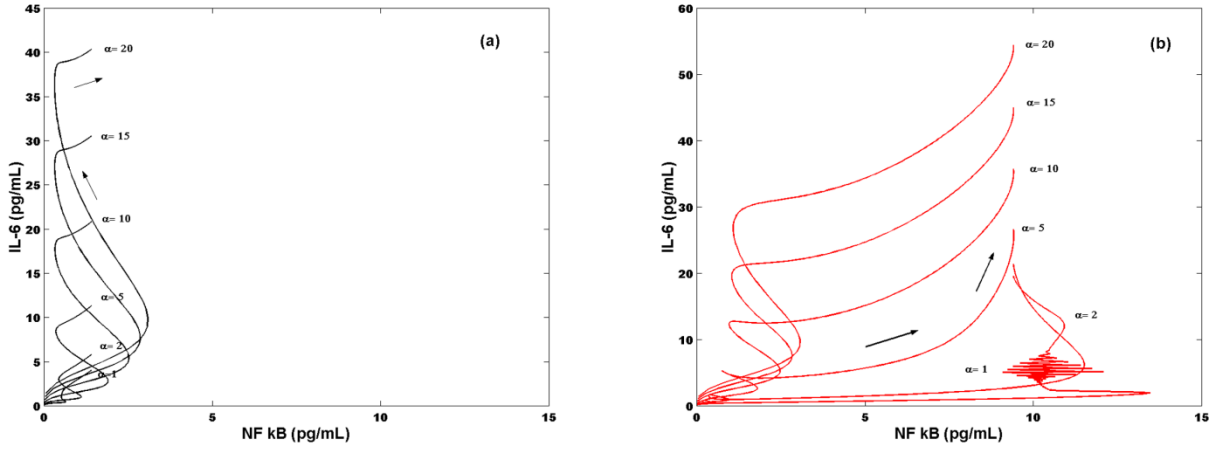

Figure SM2 5.- Effect of the variation of parameter α. a) Projection of the 10-dimensional phase space of the circuit of Figure 2 of main text on the NF κB-IL-6 phase plane for different values of the parameter $\alpha(t)$. In this Figure we show six trajectories generated from six increasing values of α, each one converging to a stable node that corresponds to a state of increasing concentration of IL-6 (from ~ 5 to ~ 40 pg mL^{-1}) in the plasma and ~ 1.4 pg mL^{-1} free NF κB. In this case all the gene translation velocities are equal to 2 pg mL^{-1} s^{-1}. b) The presence of the viral protein Nsp5 changes the position of the stable node in the NF κB-IL-6 phase plane without changing its qualitative nature. For each stable node, the concentration of free NF κB corresponds to a value of ~ 10 pg mL^{-1}, and the concentration of IL-6 changes from ~ 20 to ~ 55 pg mL^{-1}. Each node corresponds to an OSIS.

3.3) Effect of the intensity of IκB inhibition on the circuit dynamics

The parameter k_1 of the model (see Table 1 of main text) measures the intensity of the inhibition of IκB on cytoplasmic NF κB, which corresponds to the negative feedback loop of Figure 3B of main text. Figure SM2 6a shows that the variation of this parameter in absence of the virus (holding the rest of the parameters at the value indicated in Table of main text), and with gene translation rates $V_{nf}^{\max} = 10$ pg $mL^{-1}s^{-1}$, $V_{I\kappa B}^{\max} = 15$ pg $mL^{-1}s^{-1}$, $V_{IL6}^{\max} = 20$ pg $mL^{-1}s^{-1}$, and $V_{Cox2}^{\max} = 2$ pg $mL^{-1}s^{-1}$, produces a set of trajectories that converge to ARS for values of $k_1 \in [0, 0.5]$. However, for $k_1 \in (0.5, 0.8)$ the qualitative dynamical behavior of the circuit changes and each trajectory converge to a stable node. This set of nodes form a succession of points with decreasing concentrations of IL-6 between

10 and 18 pg mL^{-1}, and a increasing concentration of free NF κB between 1 to 12 pg mL^{-1} (trajectories not shown). For $k_1 \in [0.8, 0.85)$ the trajectories converge to a stable node for which IL-6 concentration is ~ 18 pg mL^{-1}m and the free NF κB concentration is ~ 12 pg mL^{-1}. For $k_1 \in [0.85, 0.88)$ a bifurcation occurs giving rise to oscillations of increasing amplitude and frequency in NF κB and IL-6 concentration, as the parameter k_1 increases its value. Finally, the circuit becomes unstable for $k_1 \in [0.85, \infty)$.

The presence of the virus drastically changes the above dynamical behavior. When $k_1 = 0$, the only possible state of the circuit is ARS (Figure SM2 6b). For $k_1 \in (0,0.4)$ the system becomes unstable. In the interval $k_1 \in [0.4, 0.69)$ each trajectory converge to a stable nodes with IL-6 concentration of 30 pg mL^{-1} and a NF κB concentration that varies from ~ 6 to 12 pg mL^{-1}. Each node represents an OSIS state. In this case, when $k_1 \in [0.69, 0.75)$ a bifurcation occurs giving rise to oscillations of increasing amplitude and frequency in NF κB and IL-6 concentration, as the parameter k_1 increases its value. In this case, the amplitude of the oscillations is larger than in absence of the virus, and the oscillations appear at a lower value of k_1. For values of $k_1 \geq 0.75$ the circuit becomes unstable.

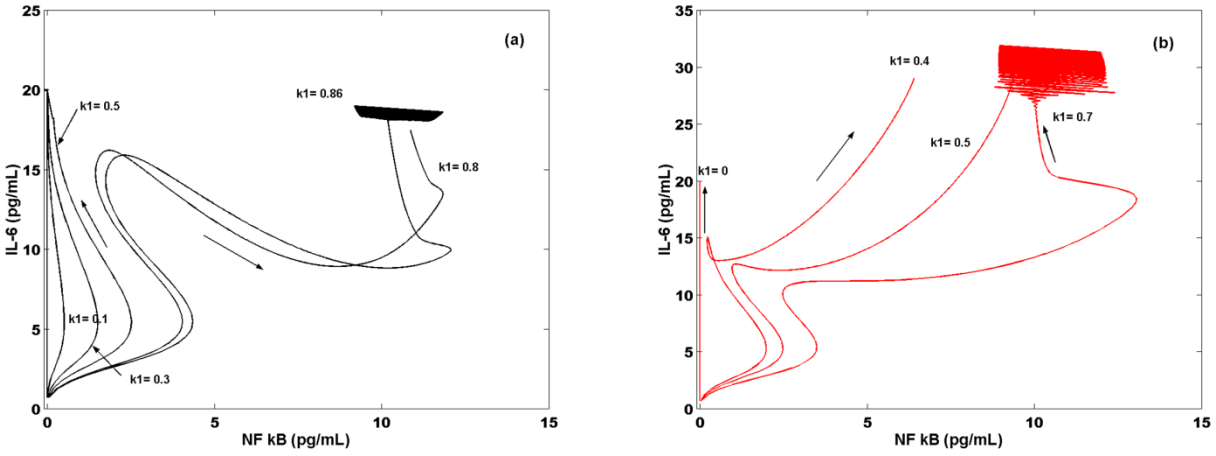

Figure SM2 6- Effect of the variation of k_1. a) In absence of the virus, and with high gene translation rates, the variation of parameter k_1 produces the modification of the qualitative dynamics of the circuit from a tendency to remain in ARS ($k_1 \leq 0.5$) to produce an oscillatory dynamics ($k_1 \in [0.8, 0.85)$). In all cases the maximum concentrations of IL-6 and free NF κB are 20 and 12 pg mL^{-1} respectively. b) In presences of the virus, in OSIS conditions, the circuit becomes unstable for $k_1 \in (0, 0.4)$. In contrast to panel (a), for each value of k_1 the trajectory converges to a node with high concentration of IL-6 (~ 30 pg mL^{-1}) when $k_1 \in [0.4, 0.69)$. Oscillations occur at a lower value of k_1 (bifurcation point at $k_1 = 0.69$) indicating a faster release of NF κB from the inhibitory effect of IκB due to the presence of Nsp5.

3.4) Effect of the diffusion rate of NF κB into the nucleus

The release of NF κB into the cytoplasm and its subsequent mobilization into the nucleus is a key step in the activation of its target genes *NF κB*, *IL-6*, *Cox2*, and *IκB*. In the model the parameter that controls this process is *D*, which in ARS has a value of 1 s^{-1}. In conditions of high translation velocities of *NF κB*, *IL-6*, *Cox2*, and *IκB* (10, 20, 2, and 15 pg mL^{-1} s^{-1}, respectively) variation in the value of this parameter in absence of the virus is indicative of the form in which the activation of the immune response depends on the localization of NF κB in the nucleus. We varied this parameter from 0 to 5 s^{-1}, holding the rest of the parameters at a constant value (Table 1 main text). We found

that when $D = 0$ exists a stable node in the NF κB-IL-6 phase plane that corresponds to a IL-6 concentration of ~ 20 pg mL^{-1}, and a NF κB concentration of ~ 5 pg mL^{-1}. In this case the concentration of NF κB in nucleus and the probability of activation of its target genes are zero. This result indicates that the mobilization of NF κB into the nucleus is a *necessary* condition to start the immune response in the circuit of Figure 2 of main text, even in the presence of an external signal $\alpha(t)$ = 10 pg $mL^{-1}s^{-1}$. For $D \in (0,5]$ the circuit enters in the ARS, and values of $D > 5$ s^{-1} destabilizes the circuit (Figure SM2 7a).

In presence of the virus, the response of the circuit to $D = 0$ is identical to the reported in panel (a), indicating that neither the external signal $\alpha(t)$ nor the virus can start the immune response if NF κB cannot be translocated into the nucleus (Figure SM2 7b). However, when $D \in (0,12)$ the presence of Nsp5 produce a series of steady responses in which IL-6 has a concentration of ~ 30 pg mL^{-1}, and NF κB decreases from ~ 8 to ~ 2 pg mL^{-1} as parameter D increases. This result indicates that the virus increases the availability of NF κB in the nucleus, promoting gene transcription in the circuit and a strong immune response (OSIS). Values of $D > 12$ s^{-1} destabilize the circuit.

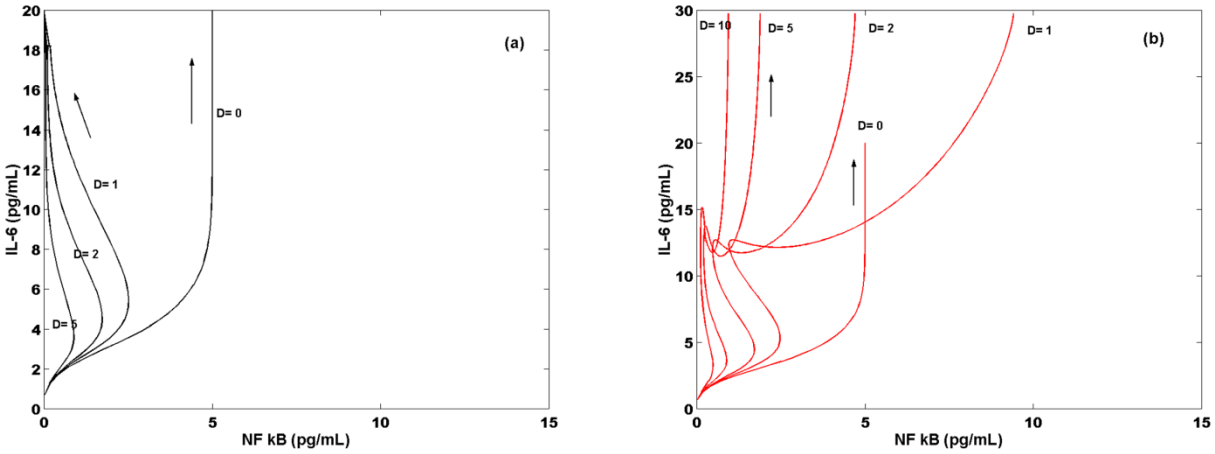

Figure SM2 7.- Effect of the variation of parameter *D*. a) In absence of movement of NF κB into the nucleus ($D = 0$) the circuit exhibits a stable node in absence of Nsp5 in which IL-6 concentration is ~ 20 pg mL^{-1} and NF κB concentration is ~ 5 pg mL^{-1} **.** For values of $D \in$ **(0,5]** the circuit enters in ARS, and values of D > 5 destabilize the circuit. b) In presence of Nsp5 (OSIS), when $D \in (0,12)$ the presence of Nsp5 produce a series of steady responses in which IL-6 has a concentration of ~ 30 pg mL^{-1}, and NF κB decreases from ~ 8 to ~ 2 pg mL^{-1} as parameter D increases.

3.5) Effect of NF κB in the nucleus

In the nucleus of the type 2 alveolar lung cells, NF κB promotes the transcription of its target genes *NF κB*, *IL-6*, *IκB* and *Cox2*. The concentration of NF κB in the nucleus is regulated by a series of mechanisms whose intensity we represent by the parameter k_{deg}, which in ARS has a value of 2 s^{-1} (Table 1 of main text). In conditions of high translation velocities of *NF κB*, *IL-6*, *Cox2*, and *IκB* (10, 20, 2, and 15 pg $mL^{-1}s^{-1}$, respectively) variation in the value of this parameter in absence of the virus is indicative of the form in which the activation of the immune response depends on the availability of NF κB in the nucleus. We varied this parameter from 0 to 5 s^{-1}, holding the rest of the parameters at a constant value (Table 1 main text). We found that when $k_{deg} = 0$ the circuit becomes unstable, indicating that the nuclear regulatory mechanisms of NF κB are necessary to produce a stable immune response. For $k_{deg} \in (0,2)$ the trajectories in the NF κB – IL-6 phase plane converge to stable

nodes for which IL-6 and cytoplasmic NF κB concentrations decrease (Figure SM2 8a). When k_{deg} = 2 s^{-1} the circuit enters in ARS, and for k_{deg} > 2 the circuit becomes unstable.

In presence of the virus, the qualitative dynamical behavior of the circuit drastically changes for k_{deg} ∈(0, 50). In this case the trajectories in the NF κB – IL-6 phase plane converge to numerous stable nodes for which IL-6 and cytoplasmic NF κB concentrations decrease as k_{deg} increases (Figure SM2 8b), indicating that Nsp5 enhances the nuclear concentration of NF κB that, in turn, produces a raise in the intensity of the inhibitory mechanisms required to regulate its activity. Each of this nodes represents an OSIS, which can be only suppressed when k_{deg} = 50 s^{-1} and the circuit enters in the ARS.

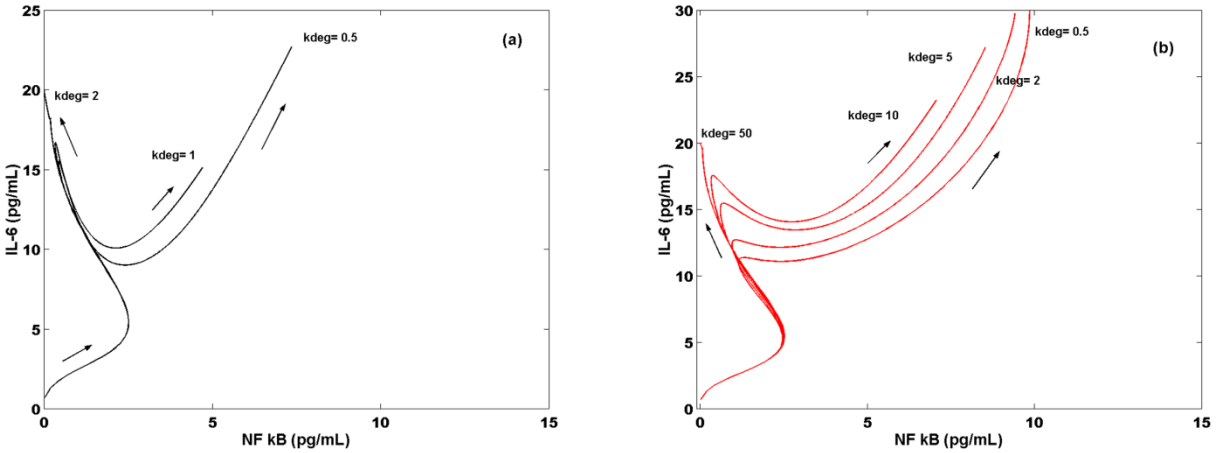

Figure SM2 8.- Effect of the variation of parameter k_{deg}. a) In conditions of high translation velocities of *NF κB*, *IL-6*, *Cox2*, and *IκB* (10, 20, 2, and 15 pg $mL^{-1}s^{-1}$, respectively) variation in the value of this parameter in absence of the virus is indicative of the form in which the activation of the immune response depends on the availability of NF κB in the nucleus. For k_{deg} ∈(0,2) each trajectory converges to a stable node for which IL-6 and cytoplasmic NF κB concentrations successively decrease. When k_{deg} = 2 s^{-1} the trajectories converges to the ARS. b) In presence of the virus, the qualitative dynamical behavior of the circuit drastically changes for k_{deg} ∈(0, 50). In this case, each trajectory converges to a stable node that represents an OSIS. When k_{deg} = 50 s^{-1} the trajectories converges to the ARS. In both panels, when k_{deg} = 0 the circuit becomes unstable